

Effect of perturbations on yield in ICF targets – 4π 3D hydro simulations

S. Taylor^a, B. Appelbe, N.P. Niasse and J.P. Chittenden

Department of Physics, Imperial College London

Abstract. ICF simulations were carried out with the amplitude of perturbations from spherical symmetry treated as a free parameter with the aim of reproducing experimentally observed yields. The simulations began at peak velocity and multi-wavelength perturbations were imposed in the velocity field. It was found that increasing the perturbation caused the gamma bang time to lag behind the xray bang time. Fluid motion broadening of the neutron spectrum was also examined. The effect of perturbation amplitude on alpha particle losses was investigated.

1. INTRODUCTION

Perturbations from spherical symmetry due to hydrodynamic instabilities are a major mechanism of yield reduction in Inertial Confinement Fusion (ICF). The extent to which these perturbations degrade target performance in the National Ignition Facility (NIF) is not fully understood, and reducing their effects is a stated stepping stone to ignition [1]. In section 2, the level of perturbation necessary to produce experimentally observed yields is assessed.

It is seen in simulations of wire-array Z-pinches that the behaviour of a perturbed pinch at stagnation differs between simulations that include all 2π of the azimuth and those that include only a portion, assuming cylindrical symmetry [2]. In the latter, spikes are met by their symmetric partners as they reach the axis and decelerate leaving a stagnated column on-axis. In the former, there is a net radial momentum at a given z and the pinch breaks apart on stagnation. A similar effect may occur in ICF, preventing the hotspot from maintaining a spherical core with a well-defined 3D radius. This would need to be accounted for in scaling studies such as [3] and [4].

Perturbations reduce yield partly by increasing the surface area of the hotspot, enhancing energy loss due to thermal conduction and alpha particle transport. In 3D, the hotspot surface area is effectively increased since perturbations are no longer correlated in the ϕ -direction. In section 3, the scaling of alpha particle confinement by the hotspot with perturbation amplitude is investigated by postprocessing perturbed hydro simulations with an alpha particle transport model [5].

2. INFLUENCE OF PERTURBATIONS ON YIELD, BANG TIME AND NEUTRON SPECTRA

Decelerating and burning ICF targets were simulated using GORGON, a parallel 3D Eulerian hydrocode. The target is assumed to be a fully-ionized ideal DT gas. Radiation losses and thermal conduction are included. Fusion and burnup is included with instantaneous local deposition of alpha particle energy. The spatial resolution of the simulations is $1\ \mu\text{m}$.

^ae-mail: st1509@imperial.ac.uk

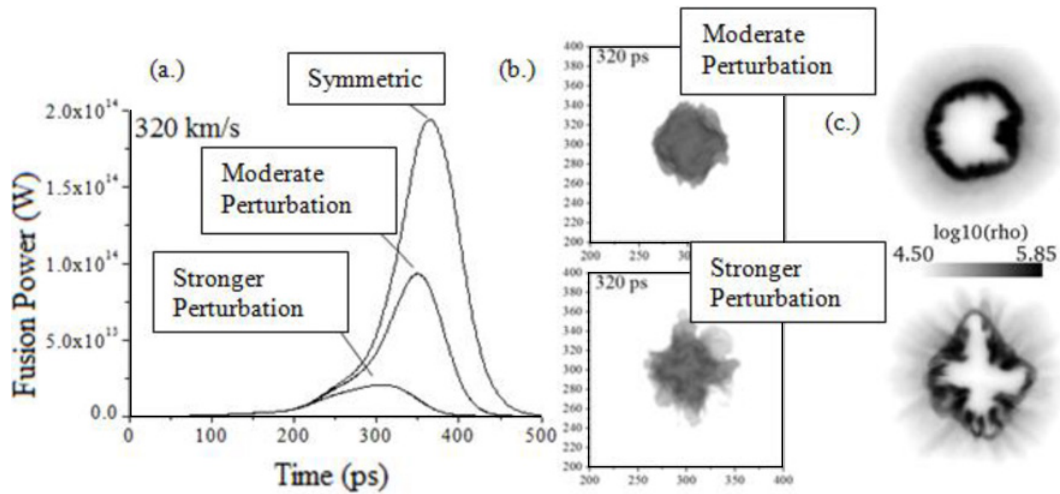


Figure 1. Burn histories of the same radial profile with various initial velocity perturbations. (b.) Soft x-ray images. (c.) Density slices.

The initial conditions are radial profiles from a 1D Lagrangian simulation of a typical NIF layered DT target taken at peak velocity [6]. The velocity profile is scaled down by 19% to match the measured value of the peak implosion velocity. By initializing at peak velocity the physics of the radiation drive can be ignored, and fewer grid points are required to resolve the target. The ablation phase perturbation must be synthesized in the initial conditions.

The perturbations are initialized using an analytic solution of the velocity field of the Rayleigh-Taylor instability (RTI) in a cylinder [7]. This field is placed at each vertex of a geodesic sphere [8]. This distribution was chosen due to its spherical symmetry. Five orders of geodisation were used, with 12 points in the zeroth order and 2564 in the fourth. The spikes' width was scaled such that they overlap, so higher orders of geodisation correspond to shorter wavelengths. The total kinetic energy of the target was kept constant. The perturbation decays exponentially from the surface of the target, to mimic the ablation-phase perturbation. The deceleration-phase RTI is seeded by the feedthrough from this. This approach is equivalent to applying an instantaneous perturbing force to the surface of a spherically symmetric target. Amplitudes of the individual spikes and the relative amplitudes of each order were set with the aim of reproducing the available experimental data.

Burn histories for three levels of perturbation are shown in Figure 1a. The typical experimental yield for this target design was $\sim 2 \times 10^{14}$ neutrons. The simulation marked 'stronger perturbation' has a yield of 8.9×10^{14} . The symmetric yield was 6.7×10^{15} , giving a yield over clean of 0.13. The bang times are earlier for the more perturbed simulations, due to the quenching of the burn causing the yield rate to drop sooner. The gamma bang time lagged behind the xray bang time more as the perturbation increased. The differences in bang times were 9.3 ps, 21 ps and 41 ps for the symmetric, moderate and stronger perturbations respectively. This is because the fusion reactivity is quenched sooner than the Bremsstrahlung emission due to its stronger temperature dependence.

Figure 1b shows false soft x-ray images of each perturbation level. At bang time, the xray image agrees qualitatively with radiographs of the most spherical NIF shots. The perturbation can be seen more clearly in the density maps, as the xray images are integrated over one spatial dimension and the emissivity depends on the electron temperature which is lower in the RTI bubbles.

Fluid motion broadening of the neutron spectrum was also observed in these simulations [9]. The neutron spectrum from thermonuclear reactions is a Gaussian centered on the neutron birth energy due to the Maxwellian distribution of the relative velocities of the reacting D and T ions – the width of

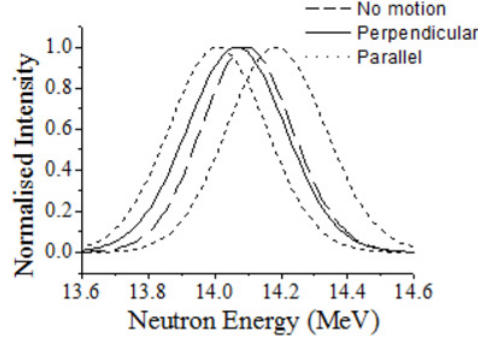


Figure 2. Neutron spectra. Solid: accounting for fluid velocity. Dashed: not accounting for fluid velocity. Dotted: in front of and behind a moving target.

the spectrum relates to the ion temperature. If the fluid has a bulk motion relative to the detector, this Gaussian is shifted. The target in Figure 2 was set to have a total average velocity of 250 km/s in a particular direction. The neutron spectrum was shifted by approximately 0.1 MeV with the detector parallel or antiparallel to the target's trajectory (dashed lines in figure 2).

In the perpendicular direction, the spectrum is not significantly shifted but is broadened due to the range of fluid velocities present in the system. The solid line shows the perpendicular neutron spectrum and the dashed line shows the spectrum calculated without taking fluid motion into account. This broadening may not be dominated by the perturbations, as some broadening would occur even in the unperturbed case. Diagnosing the ion temperature using the dashed line gives the correct value of 3.1 keV, whereas the solid line gives a value of 3.95 keV.

3. EFFECT OF PERTURBATIONS ON ALPHA PARTICLE CONFINEMENT

Alpha transport losses are increased by the perturbation because of the increased hotspot surface area and reduction of hotspot areal density by the spikes. The ratio of alpha particle energy deposited in the hotspot to that generated by fusion (χ) is expected to decrease with perturbation amplitude. This is calculated using a kinetic model of alpha transport [4] in which computational macroparticles interact with the fluid via 'classical' drag and scatter rates [10, 11]. The fluid is held stationary; this is necessary to associate a single value of χ with a single value of the perturbation amplitude. This approximation is justified by the fact that the typical lifetime of an alpha particle is around 100 times smaller than the characteristic hydrodynamic timescale.

The perturbation amplitude can be characterized using the standard deviation of (ρR) (θ, ϕ), $\sigma(\langle \rho R \rangle)$. The mean areal density also changes with perturbation amplitude; to account for this the ratio of $\sigma(\langle \rho R \rangle)$ to the mean areal density is used as the measure of perturbation amplitude. In addition to the areal density perturbation, higher perturbation amplitudes have lower hotspot temperatures. This can be accounted for by using χ/τ as the measure of the effect of perturbations on alpha confinement, where τ is the hotspot opacity to alpha particles as defined by [12]:

$$\tau = \frac{\langle \rho R \rangle \ln \Lambda}{0.0107 T_e^{3/2}}, \quad (1)$$

with T_e in keV and $\langle \rho R \rangle$ in kgm^{-2} . Note that both $\sigma(\langle \rho R \rangle)/\text{mean}(\langle \rho R \rangle)$ and χ/τ have the same dependence on $\text{mean}(\langle \rho R \rangle)$.

The kinetic calculation was carried out for several amplitudes of the first order of geodisation. The initial radial profile used in this case was data from a 1D Lagrangian simulation of an LMJ target design

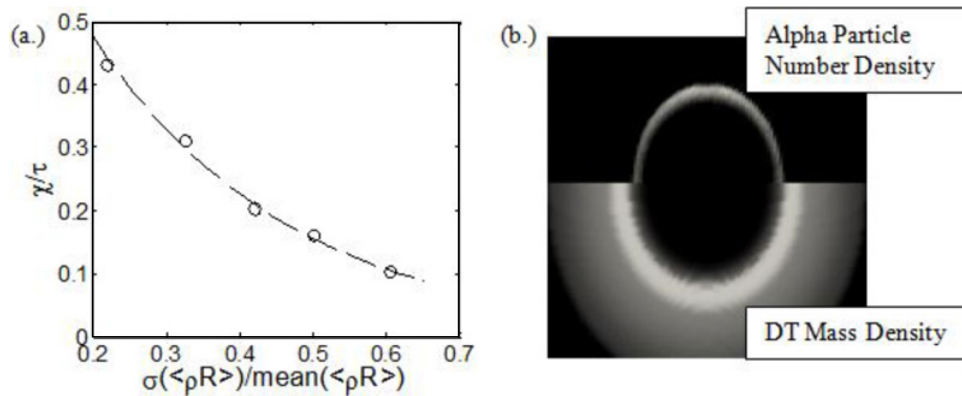


Figure 3. (a) The confinement parameter of a perturbed hotspot vs. perturbation amplitude. Dashed line: Exponential fit with an intercept of 1. (b) Top: alpha particle number density in a prolate target. Bottom: DT density. About 4/3 more alpha heating power is present at the pole.

at peak velocity. The 3D hydrocode was used to calculate the fluid properties after 550 ps, which were postprocessed with the kinetic model.

Figure 3a shows the simulated values of χ/τ vs. $\sigma(\langle \rho R \rangle) / \text{mean}(\langle \rho R \rangle)$. The data is well fit by a decaying exponential,

$$\frac{\chi}{\tau} = \exp \left[-3.71 \frac{\sigma(\langle \rho R \rangle)}{\text{mean}(\langle \rho R \rangle)} \right]. \quad (2)$$

Note that with no perturbation $\chi = \tau$. This may be due to the fact that we have defined the hotspot such that most of the alphas are generated away from the hotspot surface, so most alphas travel τl before leaving the hotspot, where l is the alpha particle range. This argument is only valid if the particle's energy deposition rate is constant, which is approximately true during the early part of the alpha particle's trajectory. In Figure 3a the hotspot surface is defined as the isochor $\rho = \rho_{max}/e^2$. If instead $\rho = \sqrt{e} \rho_{min}$ is used, the fit becomes $0.42 \exp[-3.45 \sigma(\langle \rho R \rangle) / \text{mean}(\langle \rho R \rangle)]$; in this case some alphas are generated close to the hotspot surface and do not travel τl before leaving the hotspot region.

The effect of a P2 perturbation on alpha particle transport was investigated by scaling the radial position of a spherically symmetric fluid profile by the 2nd order spherical harmonic; $r' \propto Y_2^0 r$ with $\rho(r') = \rho(r)$ and $T(r') = T(r)$. It was found that the alpha particle heating rate is greater in the extremities of these targets. This is because alpha particles are emitted with isotropically distributed velocity vectors, but there is less surface area per unit solid angle at the extremities so the alpha flux is higher.

Finally, a moderately perturbed 3D simulation was compared to a pseudo-2D simulation generated by setting the perturbation amplitude constant in the ϕ -direction. χ was $\sim 20\%$ higher in the 2D case. In the hydro simulation, the yield was $\sim 22\%$ higher in the 2D case.

References

- [1] E. I. Moses *et al.*, This Conference
- [2] J. P. Chittenden *et al.*, Plasma Phys. Control. Fusion **46**, B457 (2004)
- [3] P. Y Chang *et al.*, Phys. Rev. Lett. **104**, 135002 (2010)
- [4] R. Betti *et al.*, Phys. Plasmas **17**, 058102 (2010)
- [5] M. Sherlock, J. Comput. Phys. **227**, 2286 (2008)

- [6] M. J. Edwards, private communication (2011)
- [7] D. Layzer, *Astrophysical J.* **122**, 1 (1955)
- [8] H. Kenner, *Geodesic Math And How To Use It* (Univ. California Press, 1976)
- [9] B. Appelbe and J. P. Chittenden, *Plasma Phys. Control. Fusion* **53**, 045002 (2011)
- [10] S. Chandrasekhar, *Astrophysical J.* **227**, 255 (1955)
- [11] L. Spitzer, *Physics of Fully Ionized Gases* (Interscience, 1957)
- [12] S. Atzeni and A. Caruso, *Nuovo Cimento* **80**, 71 (1984)